Journal of Alloys and Compounds 681 (2016) 205–211

Contents lists available at ScienceDirect

Journal of Alloys and Compounds

journal homepage: http://www.elsevier.com/locate/jalcom

The effect of spin orbit interaction for superconductivity in the noncentrosymmetric superconductor $CaIrSi_3$

H.Y. Uzunok [a, b], E. İpsara [a], H.M. Tütüncü [a, b, *], G.P. Srivastava [c], A. Başoglu [a, b]

[a] Sakarya Üniversitesi, Fen-Edebiyat Fakültesi, Fizik Bölümü, 54187, Adapazarı, Turkey
[b] Sakarya Üniversitesi, BIMAYAM, Biyomedikal, Manyetik ve Yarıletken Malzemeler Araştırma Merkezi, 54187, Sakarya, Turkey
[c] School of Physics, University of Exeter, Stocker Road, Exeter, EX4 4QL, UK

ARTICLE INFO

Article history:
Received 24 March 2016
Accepted 23 April 2016
Available online 25 April 2016

Keywords:
Silicides
Density functional theory
Electronic structure
Superconducting properties
Ab initio calculations
Physical properties

ABSTRACT

We have carried out an *ab initio* study of the electronic, vibrational and electron-phonon interaction properties of the body-centred tetragonal $CaIrSi_3$ by employing the density functional theory, a linear-response formalism, and the plane-wave pseudopotential method. The electronic structure and phonon dispersion relations of this material have been analyzed with and without the inclusion of spin-orbit interaction (SOI). Our electron-phonon interaction results reveal that Si-related phonon modes are more involved in the process of scattering of electrons than the remaining phonon modes due to considerable existence of the Si 3p states near the Fermi level. By integrating the Eliashberg spectral function, the average electron-phonon coupling parameter is found to be 0.58 which compares very well with its experimental value of 0.56. Using the calculated value of λ, the superconducting critical temperature (T_c) for $CaIrSi_3$ is found to be 3.20 K which is in good accordance with its experimental value of 3.55 K. Furthermore, we have shown that the effect of SOI on the values of λ and T_c is very small.

1. Introduction

There has been special interest in studying noncentrosymmetric superconductors (NCS) [1,2], which do not possess a centre of inversion in their crystal structure. The absence of inversion symmetry in their crystal structure, along with a nontrivial antisymmetric coupling, gives rise to the interesting possibility of a superconducting state with an admixture of spin-triplet pairs. Studies on NCS have been initially stimulated by the discovery of the coexistence of antiferromagnetic order (T_N = 2.2 K) and superconductivity (T_c = 0.75 K) for $CePt_3Si$ [1]. Following this discovery, pressure-induced superconductivity has been reported for the noncentrosymmetric antiferromagnets $CeRhSi_3$ [3–6], $CeIrSi_3$ [5,7–9], $CeCoGe_3$ [10,11], and $CeIrGe_3$ [12]. These four cerium-based NCS adopt the body-centred tetragonal $BaNiSn_3$-type structure in which the lack of a mirror plane perpendicular to [001] gives rise to the Rashba-type antisymmetric coupling [1,2]. These NCS actually display exotic superconducting behaviour [3–12] and also show antiferromagnetic ordering in the vicinity of the superconducting state. These four cerium-based NCS belong to the heavy fermion systems, in which complex magnetic superconducting effects may arise from strong correlations among d and f electrons, and thus an unconventional pairing can be assumed which involves spin fluctuations. As a result, it is really difficult to select effects related to the antisymmetric spin-orbit interaction in these cerium-based NCS.

In recent years, a new family of superconducting materials has been discovered with the formula RMX_3 (R = La, Ba, Sr; M = transition metal; X = Si or Ge) [13–15] which also crystallise in the noncentrosymmetric $BaNiSn_3$-type structure. In particular, Smidman and co-workers [16] report magnetic susceptibility, specific-heat, and muon spin rotation/relaxation (μSR) measurements on $LaPtSi_3$ and $LaPdSi_3$ and conclude that $LaPtSi_3$ is a type-II superconductor with T_c = 1.52 K, whereas $LaPdSi_3$ is a type-I superconductor with T_c = 2.65 K. Furthermore, the synthesis of nine new noncentrosymmetric ternary silicide superconductors, including $CaIrSi_3$ (T_c = 3.6 K), by arc melting has been reported [17]. Following this experimental work [17], Eguchi and co-workers [18,19] have shown that $CaIrSi_3$ is nonmagnetic, fully gapped superconductor based on studies with polycrystalline samples. Thus, in contrast to the cerium-based NCS, no magnetic order exists to possibly weaken or interfere with the superconducting state.

* Corresponding author. Sakarya Üniversitesi, Fen-Edebiyat Fakültesi, Fizik Bölümü, 54187, Adapazarı, Turkey.
E-mail address: tutuncu@sakarya.edu.tr (H.M. Tütüncü).

http://dx.doi.org/10.1016/j.jallcom.2016.04.245
0925-8388/

Furthermore, normal and superconducting properties of the Rashba-type noncentrosymmetric compound $CaIrSi_3$ have been reported using crystalline samples with nearly 100% superconducting volume fraction [20]. Single crystalline samples have facilitated researches to predict various interesting phenomena as well as investigate the basic information of superconductivity, such as the gap anisotropy and the mixing ratio of the singlet and triplet components. Furthermore, the superconducting properties of $CaIrSi_3$ have been also investigated using the muon spectroscopy [21,22].

Following the experimental studies, the structural and electronic properties of $CaIrSi_3$ and $CaPtSi_3$ have been investigated theoretically by employing the full-potential linearised augmented plane wave (FLAPW) and the generalised gradient approximation of the density functional theory [23]. This theoretical work shows that the band structure pictures of $CaIrSi_3$ and $CaPtSi_3$ are similar, and the near-Fermi valence bands in these phases originate from transition metal d orbitals with an admixture of valence Si orbitals. This theoretical work further indicates that the effect of spin-orbit coupling in these compounds, especially in a small energy window around the Fermi level, is rather small. Kaczkowski and Jezierski [24] have also presented the results of calculations, within the local density (LDA) and generalised gradient approximations of the density functional theory, of the electronic and structural properties of $CaIrSi_3$ and $CaPtSi_3$. Their results for these superconductors are in agreement with previous theoretical results from the work of Bannikov and co-workers [23].

In spite of the progress made in investigating the electronic properties of $CaIrSi_3$, no experimental or theoretical works have been carried out to identify specific phonon modes that are involved in strong electron-phonon interaction for developing the BCS-type superconductivity in this noncentrosymmetric superconductor. With this in mind, we have studied the structural, electronic, vibrational and electron-phonon coupling in this compound. The structural and electronic properties of this noncentrosymmetric superconductor have been studied by using the plane wave pseudopotential method within the generalised gradient approximation of the density functional scheme with and without the inclusion of spin-orbit interaction (SOI). With these results as input, a linear response approach [25] with and without SOI is utilised to obtain phonon dispersion relations as well the phonon density of states. Then, the electron-phonon matrix elements for this noncentrosymmetric superconductor are determined using the linear response method with and without SOI [25]. Furthermore, the phonon density of states and the electron-phonon matrix elements are then used to obtain the Eliashberg spectral function [26,27] with and without SOI, from which the average electron-phonon coupling parameter is obtained. The effect of the SOI on the superconducting property has been monitored by examining the results for average electron-phonon coupling parameter and the superconducting critical temperature.

2. Method

The first-principles calculations are performed by using the *ab initio* pseudopotential method as implemented in the Quantum–Espresso package [25]. The exchange and correlation potentials were treated using the generalised gradient approximation (GGA) by Perdew–Burke–Ernzerhof [28]. The ion-electron interactions are treated by using the ultrasoft pseudopotentials [29]. Although previous theoretical calculations [23,24] indicate that the spin-orbit interaction has only negligible effect on the band structure around the Fermi energy, in our study, all calculations have been made with and without the inclusion of spin-orbit interaction for Ir and Si atoms. The wave function is expanded in plane waves, with the energy cutoff of 60 Ry and the electronic charge density is expanded in a basis cut off up to 480 Ry. The Kohn-Sham equations [30] are solved using an iterative conjugate gradient scheme to determine the total energy. Self-consistent solutions of the Kohn-Sham equations were obtained by employing a set of Monkhorst–Pack special $\boldsymbol{k}$ points [31]. An $8 \times 8 \times 8$ Monkhorst–Pack $\boldsymbol{k}$-point mesh is employed for calculating the structural properties of $CaIrSi_3$. The electronic structure and the electronic density of states are computed with $(24 \times 24 \times 24)$ Monkhorst–Pack $\boldsymbol{k}$-point mesh.

The phonon spectrum and electron-phonon coupling functions are calculated using the linear-response method [25]. We have used a $(8 \times 8 \times 8)$ grid for sampling the irreducible segment of the Brillouin zone (BZ) in our phonon calculations. In order to get the full phonon spectrum, we calculate 13 dynamical matrices on a $4 \times 4 \times 4$ grid in $\boldsymbol{q}$ space. Finally, these dynamical matrices are Fourier transformed to get the full phonon spectrum and density of states. The technique for the calculation of the electron–phonon coupling has been well described in our previous work [32] and will not be repeated here. We only mention that the Fermi-surface sampling for the evaluation of the electron-phonon matrix elements was carried out by using the $24 \times 24 \times 24$ $\boldsymbol{k}$-mesh with a Gaussian width 0.02 Ry. The Eliashberg spectral function was also computed using this $\boldsymbol{k}$-mesh.

3. Results

3.1. Structural and electronic properties

$CaIrSi_3$ adopts a body-centred tetragonal $BaNiSn_3$-type crystal structure, with space group *I4mm* (no. 107) and one formula unit per primitive unit cell. The five atoms inside a primitive unit cell can be classified as four non-equivalent crystallographic sites: Ca, Ir, Si1, and Si2 according to the symmetry. The atomic positions are: Ca (2a) (0, 0, 0), Ir (2a) (0, 0, z_{Ir}), Si1 (2a) (0, 0, z_{Si1}), and Si2 (4b) (0, 1/2, z_{Si2}), (1/2, 0, z_{Si2}). Thus, this body-centred tetragonal structure is characterised by two lattice parameters (a and c) and three internal parameters (z_{Ir}, z_{Si1} and z_{Si2}). The equilibrium values of the lattice parameters and internal parameters are obtained under the conditions of the minimum of the total energy and vanishing forces on the atoms. The bulk modulus (B) and its pressure derivative (B') have been computed by minimising the crystal total energy for different values of crystal volume by means of Murnaghan equation of state [33]. The calculated equilibrium lattice parameters (a and c), the volume of primitive unit cell (V), internal parameters (z_{Ir}, z_{Si1} and z_{Si2}), bulk modulus (B) and its pressure derivative (B') with and without SOI are presented in Table 1, together with previous theoretical [23,24] and experimental [18,21] results for comparison. As can be seen from this table, the effect of SOI on the structural properties of $CaIrSi_3$ is very small. Our results for a and c with SOI are only 0.4% and 0.5% different from the recent experimental values [21] of 4.196 Å and 9.871 Å. Similarly, our results for z_{Ir}, z_{Si1} and z_{Si2}, with SOI, are within 0.1%, 0.1% and 0.2% of the experimental values [18]. However, to the best of our knowledge, experimental data do not exist for the bulk modulus and its pressure derivative. Fig. 1 presents the illustration of the tetragonal structure of using the structural parameters from Table 1. The crystal structure has no mirror plane perpendicular to the $z-$ axis. Each Ir atom coordinates with four basal Si2 atoms and one apical Si1 atom. The values of the bond lengths with SOI are found to be 2.360 Å for the Ir-Si1 bond and 2.382 Å for the Ir-Si2 bond. These interatomic distances are considerably shorter than the value of 2.520 Å determined from the summation of the atomic radii: 1.41 Å for Ir and 1.11 Å for Si. This result is the evidence of strong covalent bonds between Ir atom and Si atoms. Each Si1 atom coordinates to four Si2 atoms with the

Table 1
The calculated structural parameters with and without spin-orbit interaction (SOI) for $CaIrSi_3$ and their comparison with available experimental and theoretical results.

Source	a (Å)	c (Å)	V (Å^3)	z_{Ir}	z_{Si1}	z_{Si2}	B (GPa)	B′
This work with SOI	4.213	9.918	88.019	0.6473	0.4093	0.2594	108.3	4.22
This work without SOI	4.215	9.915	88.076	0.6455	0.4073	0.2579	108.0	4.34
GGA [23]	4.160	10.164	87.947	0.6416	0.4096	0.2589		
GGA [24]	4.214	9.909	87.981	0.6469	0.4082	0.2595		
LDA [24]	4.159	9.779	84.575	0.6469	0.4087	0.2593		
Experimental [18]	4.183	9.872	86.368	0.6467	0.4098	0.2589		
Experimental [21]	4.196	9.871	86.896					

interatomic distance of 2.591 Å which is longer than the corresponding value of 2.352 Å in the diamond-structure Si, thus suggesting the existence of weaker Si-Si bond as compared to that in the Si crystal.

The calculated energy-band structures with and without SOI, at the equilibrium volume for $CaIrSi_3$, along the high-symmetry lines in the body centred tetragonal Brillouin zone (BZ) are illustrated in Fig. 2. The overall band profiles compare very well with previous theoretical results [23,24]. The electronic structures both with and without SOI exhibit the metallic character of this non-centrosymmetric superconductor, with at least one band crossing the Fermi level along Γ-G1, G1-Z, Γ-X, P-Γ, Γ-N, N-P and P-Z. On the other hand, the valence and conduction bands are well separated from each other along the Z-Γ and X-P symmetry directions. A

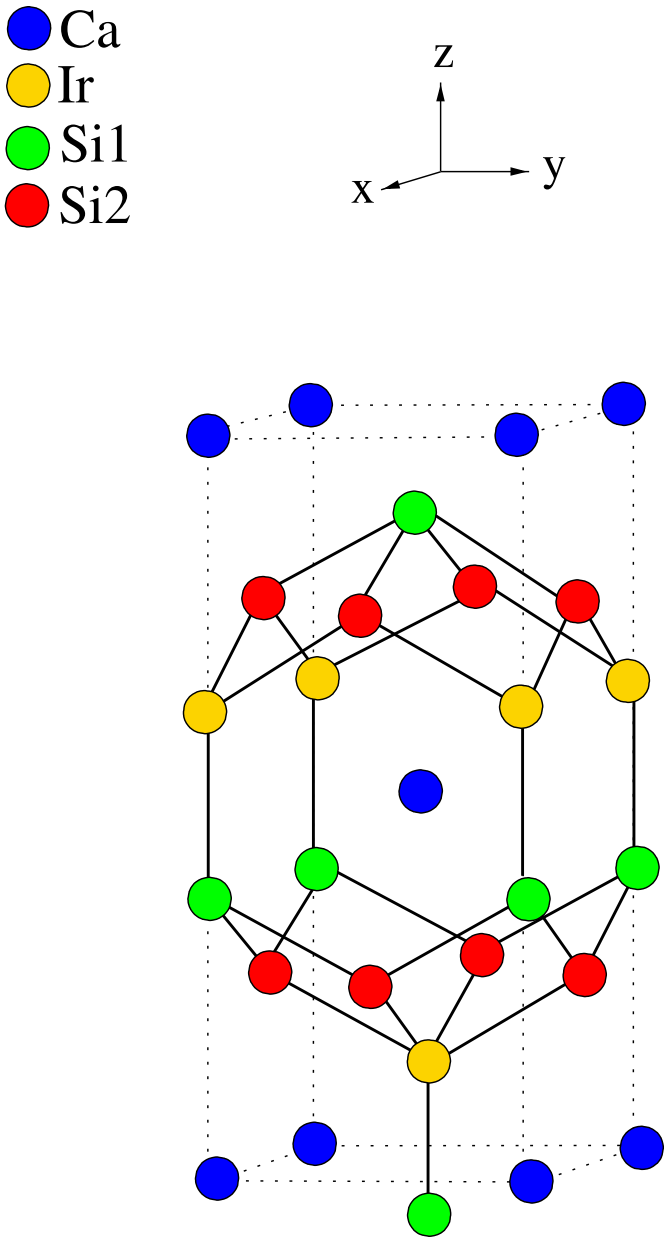

Fig. 1. The $BaNiSn_3$-type crystal structure of $CaIrSi_3$. The crystal structure has no mirror plane perpendicular to the z-axis.

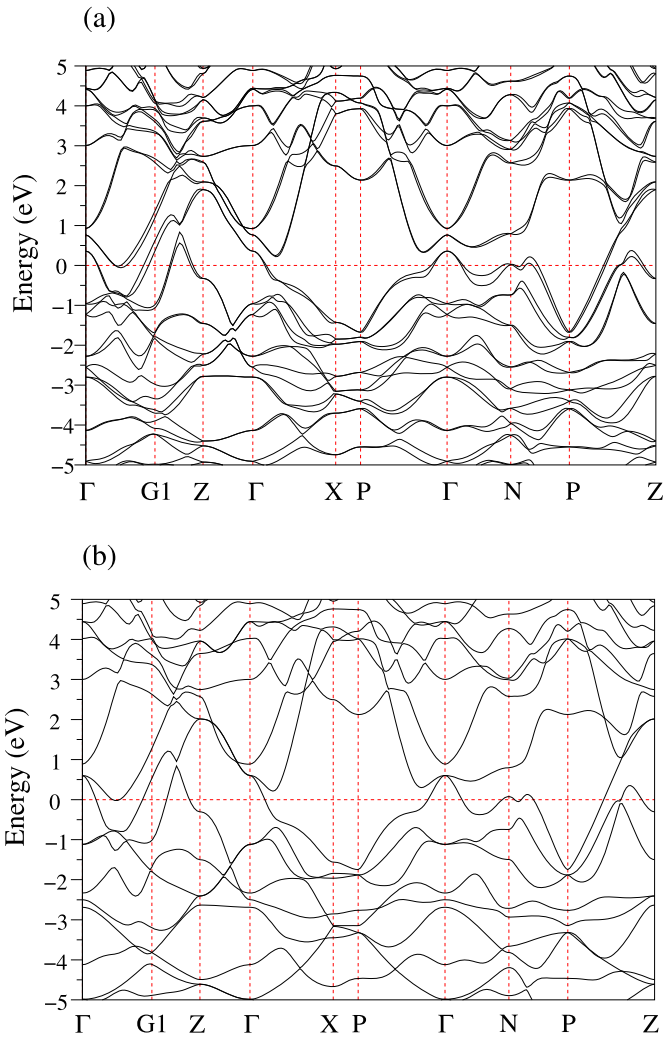

Fig. 2. The electronic band structure for $CaIrSi_3$ (a) with SOI and (b) without SOI. The energy zero is set at the Fermi level. The high-symmetry points in the irreducible Brillouin zone in cartesian coordinates are: G1 = $2\pi/a((1/2 + a^2/2c^2)$, 0.00, 0.00), Z = $2\pi/a$(0.00, 0.00, a/c), X = $2\pi/a$(0.50, 0.50, 0.00), P = $2\pi/a$(0.50, 0.50, $a/2c$), and N = $2\pi/a$(0.0, 0.50, $a/2c$). Note that G1 is the zone boundary in the [100] direction.

comparison between Fig. 2(a) and (b) shows that the inclusion of SOI has split several bands. Of particular interest is to note that there is a clear, but small, splitting of bands in the window of ±0.5 eV around the Fermi energy, with the maximum of 200 meV splitting between the first pair of bands just below the Fermi energy along the Γ–N direction. This may be the first sign that a mixing of the spin-singlet and spin-triplet components in the superconducting condensate is weak and the spin-singlet Cooper pairs dominate.

In order to reveal the atomic orbital origin of the electronic structure, we have calculated the total and the angular momentum decomposition of the atom projected density of states (DOS). The total density of states (DOS) and the partial density of states (PDOS) with SOI are presented in Fig. 3. As can be seen from this figure, the Ir 5d and Si 3p orbitals make significant contributions in a small the energy range below and above the Fermi level. In contrast, in the same energy window the partial DOS of the Ca 3d orbital is comparatively less significant. This picture is expected because Ca atoms are nearly in the charge state close to Ca^{2+}. This means that Ca atoms are bonded with the other atoms mainly by ionic interactions. The DOS features below −5.9 eV arise from strongly hybridised Si1 and Si2 electronic states, which is indicative of covalent Si1-Si2 interaction. For energy window from −5.9 to −1.6 eV, there is high degree of hybridisation of Ir 5d states with Si1 3p and Si2 3p states, signifying covalent interaction between Ir and Si atoms. Thus, the analysis based on the electronic DOS reveals that the bonding nature in $CaIrSi_3$ is a combination of covalent, ionic and metallic bonds. The total density of states at the Fermi level ($N(E_F)$) with SOI is computed to be 1.94 States/eV, which compares well with the previous GGA value of 1.98 States/eV [23]. The value of ($N(E_F)$) without SOI is found to be 1.91 States/eV, which is slightly lower than the result with SOI. This result may be the second sign that a mixing of the spin-singlet and the spin-triplet components in the superconducting condensate is weak and the spin-singlet Cooper pairs dominate. We have to mention that a similar observation has been made in previous theoretical calculations [23,24]. Our computed value of $N(E_F)$ with SOI is composed of roughly 13% Ca 3d, 21% Ir 5d, 12% Ir 6p, 19% Si1 3p and 27% Si2 3p states. This picture reveals that the p electrons of Si1 and Si2 atoms make significant contribution to the superconducting properties of $CaIrSi_3$ since Cooper pairs in the BSC theory are formed by electrons which have energies close to the Fermi level.

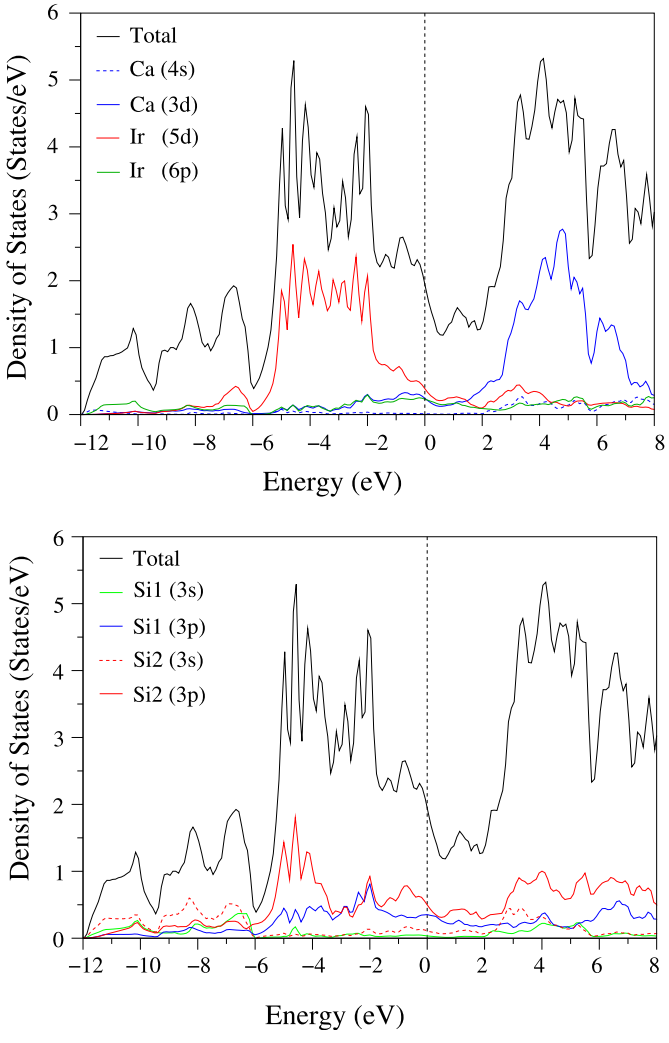

Fig. 3. The total and partial electronic density of states for $CaIrSi_3$, calculated with SOI included.

3.2. Phonons and electron-phonon interaction

The zone-centre phonons for $CaIrSi_3$ can be classified by the irreducible representation of the point group C_{4v}. As obtained from the group theory, the symmetries of the optical phonon modes can be expressed as:

$$\Gamma(\text{optical}) = 4E + 3A_1 + B_2,$$

with the B, A and E modes being singly, singly and doubly degenerate representations, respectively. The one-dimensional *A* and *B* modes consist of atomic vibrations along the ***z*** direction while the doubly degenerate E modes consist of atomic vibrations in the ***x***–***y*** plane. The frequencies of the zone-centre phonon modes are presented along with their electron-phonon coupling parameters and their mode activities in Table 2. This table clearly shows that the effect of SOI on the phonon frequencies and their electron-phonon coupling parameters is very small. Thus, we will present our phonon dispersion and electron-phonon interaction results with SOI. It is worth mentioning that the electron-phonon coupling parameters of the second higher E, the B_1 and the highest A_1 phonon modes are larger than the corresponding parameters for the remaining phonon modes. The eigendisplacements of these phonon modes are shown Fig. 4. This E mode at 5.01 THz arises from the vibrations of half the number of Si2 atoms against the in-phase vibrations of the Ca atoms with the other half the number of Si2 atoms. The B_1 mode at 7.57 THz arises from the vibrations of one layer of Si2 atoms against the vibrations of the next layer of Si2 atoms. The A_1 mode at 10.84 THz arises from the Si1 atomic layer vibrating against the Si2 atomic layer. Clearly thus, on the whole it is the Si2 atoms that make the largest contribution to the electron-phonon coupling. At this point we remind ourselves that the largest contribution to the total electronic density of states at the Fermi level also comes from Si2 3p electronic orbitals. Also, we note that in contrast to the Si1 atoms, the Si2 atoms (sandwiched between Si1 and Ir atomic layers) are a layer apart from the Ca atomic layer.

Up to now, we have only presented the zone-centre phonon modes. Full understanding and a trustworthy calculation of the electron-phonon coupling requires the knowledge of the complete phonon dispersion relations throughout the Brillouin zone. The calculated phonon dispersion relations along the selected high symmetry directions for the body-centred tetragonal $CaIrSi_3$ are depicted in Fig. 5(a). With five atoms in the primitive unit cell, there are twelve optical phonon branches. As a result of group symmetrical degeneracies, however, the number of phonon branches is

Table 2
Calculated zone-centre phonon frequencies (ν in THz) and the corresponding electron-phonon coupling parameters (λ) with and without spin-orbit interaction (SOI) for $CaIrSi_3$. R and IR indicate Raman-active and infrared-active vibrations, respectively.

Mode	E	A_1	E	E	B_1	A_1	A_1	E
ν with SOI	4.08	4.99	5.01	7.50	7.57	9.36	10.84	11.24
ν without SOI	4.11	4.98	5.05	7.45	7.71	9.39	10.87	11.19
λ with SOI	0.044	0.070	0.104	0.068	0.153	0.080	0.150	0.021
λ without SOI	0.042	0.076	0.108	0.070	0.154	0.086	0.160	0.022
Active	IR + R	IR + R	IR + R	IR + R	R	IR + R	IR + R	IR + R

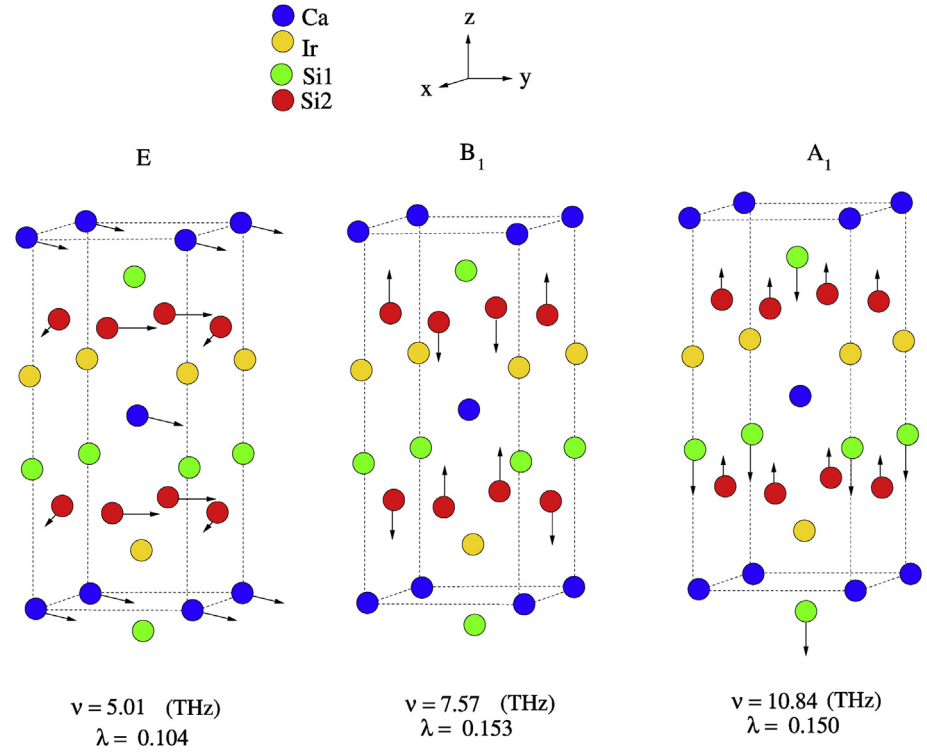

Fig. 4. Eigenvector representations of the zone-centre second E, B_1 and highest A_1 phonon modes in $CaIrSi_3$.

reduced to ten along the Γ-Z symmetry direction. The total and partial phonon density of states are shown in Fig. 5(b). The frequency region below 4.3 THz consists of the acoustical and optical vibrations of all atoms with maximum contribution coming from Si atoms. As Ca is the lightest element in this material, one can expect that these atoms dominate at higher frequencies. However, the contribution of Ca atoms is strongest between 4.3 and 5.2 THz, being negligible above 6.3 THz. Such low frequencies of calcium vibrations confirm rather weak bonding forces between this light mass atom and other atoms. The partial DOS reveals a significant Si1–Si2 hybridisation above the first gap region. The Si-related features are found over the whole range of the phonon frequencies. This knowledge, together with the previously mentioned nature of the electronic density of states near the Fermi energy, clearly suggest that Si p electron states and Si-relevant phonon modes are crucial for the development of BCS-type superconductivity in $CaIrSi_3$.

The three acoustic phonon modes are also involved in the process of scattering of electrons as are the zone-centre optical phonon modes. In order to show the contribution of acoustic phonon branches to the average electron-phonon coupling parameter, we illustrate the frequency-dependent electron-phonon coupling parameters of the three acoustic phonon branches along the Γ-N direction in Fig. 6. The most notable feature of this figure is that the electron-coupling parameter of these acoustic branches rapidly increases as their wave vector approaches the zone centre along the Γ-N direction. The rapid decrease in their electron-phonon coupling parameters away from the zone centre can be related to the strong increase in their phonon frequencies. According to the McMillan-Hopfield expression, the electron-phonon coupling constant (λ) can be presented in the following form [26,27].

$$\lambda = \frac{N(E_F)\langle I^2\rangle}{M\langle\omega^2\rangle}, \tag{1}$$

where M shows the average atomic mass and $<\omega^2>$ is the average of squared phonon frequencies. Further, $<I^2>$ represents the Fermi surface average of squared electron-phonon coupling interaction. According to the above equation, the value of electron-phonon coupling constant (λ) decreases rapidly with increasing phonon frequency.

In order to investigate the strengths with which different modes of atomic motion couple to the electrons at the Fermi energy, and thereby are skillful in affecting the superconducting properties of $CaIrSi_3$ most, we have illustrated the Eliashberg function $\alpha^2 F(\omega)$ and the electron-phonon coupling parameter $\lambda(\omega)$ together in Fig 7. This figure indicates that the value of average electron-phonon coupling parameter (λ) for this superconductor is 0.58. This value

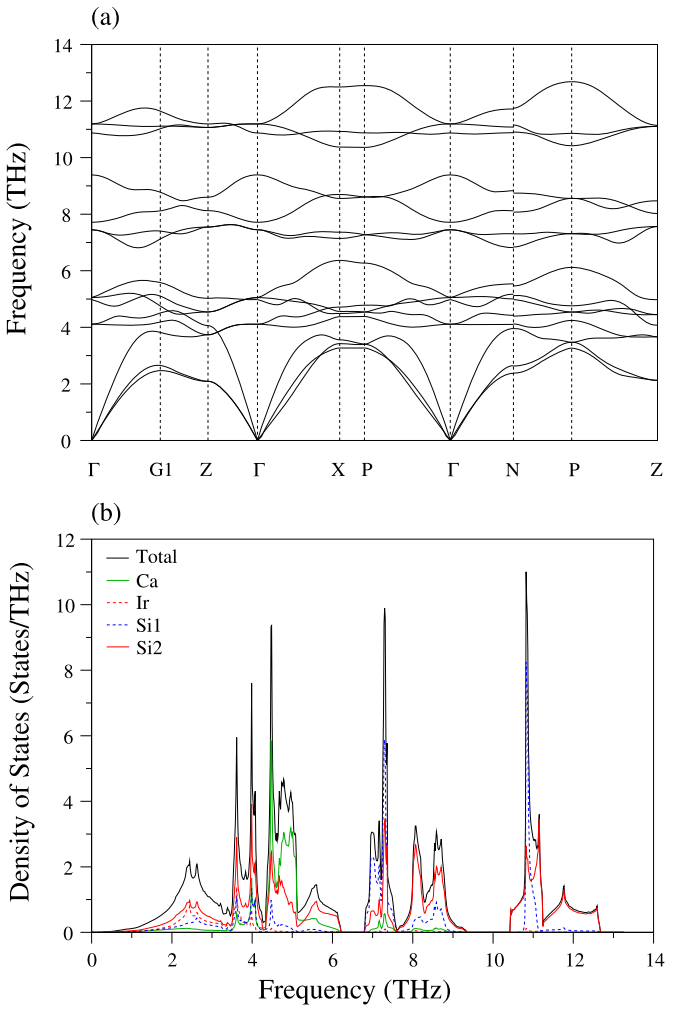

Fig. 5. (a) Calculated phonon spectrum for $CaIrSi_3$ along symmetry lines of the body-centred tetragonal Brillouin zone. (b) The total and partial phonon density of states in $CaIrSi_3$.

is in excellent agreement with the experimentally deduced value of 0.56 [20]. With this result, we can emphasize that the electron-phonon interaction in this superconductor is of weak strength. The average electron-phonon coupling parameter can be utilised to obtain the electronic specific-heat coefficient ($\gamma = \gamma_{bs}(1 + \lambda)$), which is renormalised by the phonon enhancement factor $(1 + \lambda)$ compared to its band structure value $\left(\gamma_{bs} = \frac{\pi^2 k_B^2 N(E_F)}{3}\right)$. From our calculations, the value of γ is found to be 7.2 mJ/mol K^2, which can be fairly compared with 6.6 mJ/mol K^2 in the experimental work of Eguchi and co-workers [20]. Furthermore, the average electron–phonon coupling constant λ can be used to calculated the logarithmically averaged phonon frequency $\omega_{\ln}$ which is given as

$$\omega_{ln} = \exp\left(2\lambda^{-1}\int_0^{\infty}\frac{d\omega}{\omega}\alpha^2F(\omega)\ln\omega\right). \quad (2)$$

From the above equation, the value of logarithmically averaged phonon frequency $\omega_{\ln}$ is found to be 229.14 K. Finally the values of λ and $\omega_{\ln}$ can be used to determine the superconducting transition temperature T_c using the Allen-Dynes modification of the McMillian equation [26,27].

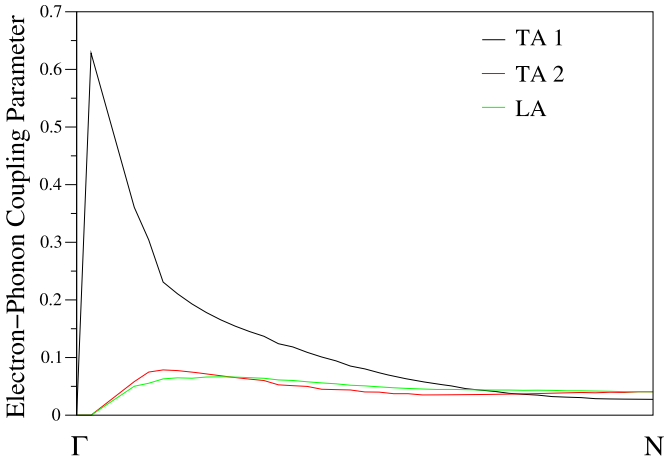

Fig. 6. The calculated wavevector-dependent electron-phonon coupling parameter first transverse acoustic branch (TA_1), second transverse acoustic branch (TA_2) and longitudinal acoustic branch (LA) along the Γ-N direction in $CaIrSi_3$.

$$T_c = \frac{\omega_{\ln}}{1.2}\exp\left(-\frac{1.04(1+\lambda)}{\lambda-\mu^*(1+0.62\lambda)}\right), \quad (3)$$

where μ^* is an effective screened Coulomb repulsion constant. With the acceptable choice $\mu^* = 0.13$, the superconducting transition temperature T_c is found to be 3.20 K, which compares very well with the recent experimental value of 3.55 K [22]. We have to note that the values of λ, γ, $\omega_{\ln}$ and T_c without SOI are found to be 0.57, 7.10 mJ/mol K^2, 231.42 K and 3.10 K, which are very close to their corresponding values of 0.58, 7.20 mJ/mol K^2, 229.14 K and 3.20 K with SOI. This result may be the third sign that a mixing of the spin-singlet and the spin-triplet components in this superconducting condensate is weak and the spin-singlet Cooper pairs dominate.

4. Summary and conclusion

Using *ab initio* pseudopotential calculations with and without the inclusion of spin-orbit interaction (SOI), we have systemically investigated the structural, electronic, vibrational, and electron-phonon interaction properties of the noncentrosymmetric superconductor $CaIrSi_3$ with the body-centred tetragonal $BaNiSn_3$-type

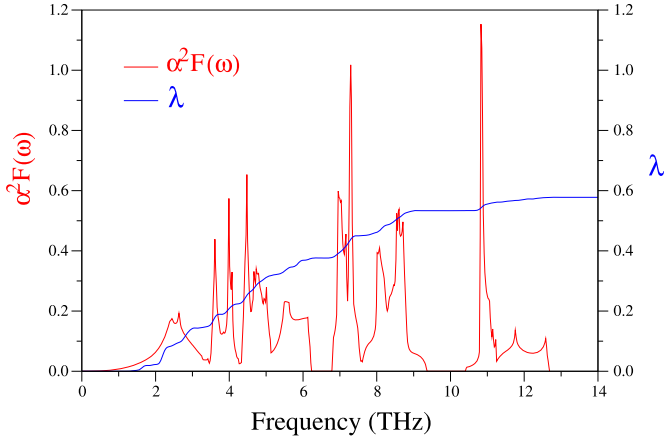

Fig. 7. The calculated electron-phonon spectral function α^2 F(ω) (red line) and the variation of the electron-phonon coupling parameter (blue line) with increasing frequency in $CaIrSi_3$. (For interpretation of the references to colour in this figure legend, the reader is referred to the web version of this article.)

structure. The calculated structural parameters with and without SOI for this noncentrosymmetric superconductor are found in agreement with available experimental and theoretical results. Our structural and electronic results reveal that the bonding in $CaIrSi_3$ can be categorised as a mixture of metallic, ionic and covalent contributions. The electronic density of states at the Fermi energy is largely constructed by Si 3p and Ir 4d orbitals.

A detailed examination of the phonon density of states shows that Si-related vibrations occur over the whole range of phonon frequencies in this system. Our electron-phonon interaction results reveal that Si-related modes are more significantly involved in the process of scattering of electrons than the remaining phonon modes due to significant existence of the Si p states near the Fermi level.

The Eliashberg spectral function is calculated by using the phonon density of states and the electron-phonon matrix elements. From the integration of this function, the value of the average electron-phonon coupling parameter is found to be 0.58, suggesting a weak strength of electron-phonon interaction in this compound. Inserting the value of average electron-phonon coupling parameter in the Allen-Dynes modification of the McMillian formula, with the screened Coulomb pseudopotential parameter $\mu^* = 0.13$, the superconducting temperature T_c is determined to be 3.20 K, which is in good accordance with its recent experimental value of 3.55 K.

Finally, we have shown that the effect of SOI on the vibrational and electron-phonon interaction properties of $CaIrSi_3$ is very small because the spin-orbit interaction has only negligible effect on the band structure around the Fermi energy.

Acknowledgement

This work was supported by the Scientific and Technical Research Council of Turkey (TÜBİTAK) (Project Number MFAG-115F135). Some of the calculations for this project were carried out using the computing facilities on the Intel Nehalem (i7) cluster (ceres) in the School of Physics, University of Exeter, United Kingdom.

References

[1] E. Bauer, G. Hilscher, H. Michor, Ch Paul, E.W. Scheidt, A. Gribanov, Yu Seropegin, H. Noël, M. Sigrist, P. Rogl, Phys. Rev. Lett. 92 (2004) 027003.
[2] E. Bauer, M. Sigrist, Non-centrosymmetric Superconductors: Introduction and Overview, Lecture Notes in Physics, Springer-Verlag, Berlin, 2012.
[3] N. Kimura, K. Ito, K. Saitoh, Y. Umeda, H. Aoki, T. Terashima, Phys. Rev. Lett. 95 (2005) 247004.
[4] N. Kimura, K. Ito, H. Aoki, S. Uji, T. Terashima, Phys. Rev. Lett. 98 (2007) 197001.
[5] Y. Tada, N. Kawakami, S. Fujimoto, Phys. Rev. B 81 (2010) 104506.
[6] N. Egetenmeyer, J.L. Gavilano, A. Maisuradze, S. Gerber, D.E. MacLaughlin, G. Seyfarth, D. Andreica, A. Desilets-Benoit, A.D. Bianchi, Ch Baines, R. Khasanov, Z. Fisk, M. Kenzelmann, Phys. Rev. Lett. 108 (2012) 177204.
[7] I. Sugitani, Y. Okuda, H. Shishido, T. Yamada, A. Thamizhavel, E. Yamamoto, T.D. Matsuda, Y. Haga, T. Takeuchi, R. Settai, Y. Önuki, J. Phys. Soc. Jpn. 75 (2006) 043703.
[8] H. Mukuda, T. Fujii, T. Ohara, A. Harada, M. Yashima, Y. Kitaoka, Y. Okuda, R. Settai, Y. Önuki, Phys. Rev. Lett. 100 (2008) 107003.
[9] H. Mukuda, T. Ohara, M. Yashima, Y. Kitaoka, R. Settai, Y. Önuki, K.M. Itoh, E.E. Haller, Phys. Rev. Lett. 104 (2010) 017002.
[10] R. Settai, I. Sugitani, Y. Okuda, A. Thamizhavel, M. Nakashima, Y. Önuki, H. Harima, J. Magn. Magn. Mater. 310 (2007) 844.
[11] M. Smidman, D.T. Adroja, A.D. Hillier, L.C. Chapon, J.W. Taylor, V.K. Anand, R.P. Singh, M.R. Lees, E.A. Goremychkin, M.M. Koza, V.V. Krishnamurthy, D.M. Paul, G. Balakrishnan, Phys. Rev. B 88 (2013) 134416.
[12] F. Honda, I. Bonalde, S. Yoshiuchi, Y. Hirose, T. Nakamura, K. Shimizu, R. Settai, Y. Önuki, Phys. C 470 (2010) S543.
[13] E. Bauer, R.T. Khan, H. Michor, E. Royanian, A. Grytsiv, N. Melnychenko-Koblyuk, P. Rogl, D. Reith, R. Podloucky, E.-W. Scheidt, W. Wolf, M. Marsman, Phys. Rev. B 80 (2009) 064504.
[14] R. Ribeiro-Palau, R. Caraballo, P. Rogl, E. Bauer, I. Bonalde, J. Phys. Condens. Matter 26 (2014) 235701.
[15] F. Kneidinger, L. Salamakha, E. Bauer, I. Zeiringer, P. Rogl, C. Blaas-Schenner, D. Reith, R. Podloucky, Phys. Rev. B 90 (2014) 024504.
[16] M. Smidman, A.D. Hillier, D.T. Adroja, M.R. Lees, V.K. Anand, R.P. Singh, R.I. Smith, D.M. Paul, G. Balakrishnan, Phys. Rev. B 89 (2014) 094509.
[17] S. Oikawa, M. Nohara, H. Takagi, in: Presented at the 63rd JPS Fall Meeting, 2008, p. 23 pQC1.
[18] G. Eguchi, D.C. Peets, M. Kriener, Y. Maeno, E. Nishibori, Y. Kumazawa, K. Banno, S. Maki, H. Sawa, Phys. Rev. B 83 (2011) 024512.
[19] G. Eguchi, F. Kneidinger, L. Salamakha, S. Yonezawa, Y. Maeno, E. Bauer, J. Phys. Soc. Jpn. 81 (2012) 074711.
[20] G. Eguchi, H. Wadati, T. Sugiyama, E. Ikenaga, S. Yonezawa, Y. Maeno, Phys. Rev. B 86 (2012) 184510.
[21] R.P. Singh, A.D. Hillier, D. Chowdhury, J.A.T. Barker, D. McK. Paul, M.R. Lees, G. Balakrishnan, Phys. Rev. B 90 (2014) 104504.
[22] Benjamin A. Frandsen, Sky C. Cheung, Tatsuo Goko, Lian Liu, Teresa Medina, Timothy S.J. Munsie, Graeme M. Luke, Peter J. Baker, P. Marco, S. Jimenez, Gaku Eguchi, Shingo Yonezawa, Yoshiteru Maeno, Yasutomo J. Uemura, Phys. Rev. B 91 (2015) 014511.
[23] V.V. Bannikov, I.R. Shein, A.L. Ivanovskii, JETP Lett. 92 (2010) 343.
[24] J. Kaczkowski, A. Jezierski, J. Alloys Compd. 506 (2011) 6142.
[25] P. Giannozzi, S. Baroni, N. Bonini, M. Calandra, R. Car, C. Cavazzoni, D. Ceresoli, G.L. Chiarotti, M. Cococcioni, I. Dabo, A.D. Corso, S. de Gironcoli, S. Fabris, G. Fratesi, R. Gebauer, U. Gerstmann, C. Gougoussis, A. Kokalj, M. Lazzeri, L. Martin-Samos, N. Marzari, F. Mauri, R. Mazzarello, S. Paolini, A. Pasquarello, L. Paulatto, C. Sbraccia, S. Scandolo, G. Sclauzero, A.P. Seitsonen, A. Smogunov, P. Umari, R.M. Wentzcovitch, J. Phys. Condens. Matter 21 (2009) 395502.
[26] P.B. Allen, Phys. Rev. B 6 (1972) 2577.
[27] P.B. Allen, R.C. Dynes, Phys. Rev. B 12 (1975) 905.
[28] J.P. Perdew, K. Burke, M. Ernzerhof, Phys. Rev. Lett. 77 (1996) 3865.
[29] A.M. Rappe, K.M. Rabe, E. Kaxiras, J.D. Joannopoulos, Phys. Rev. B 41 (1990) 1227.
[30] W. Kohn, L.J. Sham, Phys. Rev. 140 (1965) A1133.
[31] H.J. Monkhorst, J.D. Pack, Phys. Rev. B 13 (1976) 5188.
[32] H.M. Tütüncü, H.Y. Uzunok, Ertuğrul Karaca, G.P. Srivastava, S. Özer, Ş. Uğur, Phys. Rev. B 92 (2015) 054510.
[33] F.D. Murnaghan, Proc. Natl. Acad. Sci. U. S. A. 50 (1944) 697.